

Silver Formation, Particle Size Distribution, and Morphology in Photothermographic Systems

Mark B. Mizen[▲]

The Antioch Company, St. Cloud, Minnesota

Spectroscopic measurements of photothermographic systems at development temperatures show how Ag particles form during the course of the development process. In standard systems, development follows autocatalytic kinetics. Systems containing infectious developers exhibit more unusual kinetics which do not generally fit simple mathematical models. In standard photothermographic systems, Ag particles have a median diameter of approximately 0.065 μm . The median diameter is reduced to 0.028 μm and the particles are generally more spherical in the presence of an infectious developer. Intermediate sizes and morphologies are possible with low levels of infectious development. Particle size and morphology correlates to light absorption and Ag covering power. Standard photothermographic development proceeds sequentially, while infectious development occurs in parallel.

Journal of Imaging Science and Technology 43: 528–534 (1999)

Introduction

Photothermographic systems, such as DryViewTM or DryView ImagesettingTM from Imation Corp., contain all required components in the final construction.^{1,2} Processing with a hot roll (DryView) or flatbed (DryView Imagesetting) typically requires about 15 s at 122°C. These photothermographic films, reviewed by Klosterboer,³ use light-sensitive Ag halide sensitized for 800 nm laser exposure to catalyze the reduction of light insensitive Ag compounds, such as long-chain Ag carboxylates (Ag soap), $[\text{Ag}(\text{O}_2\text{CR})]_2$, $\text{R} = \text{C}_{17}\text{H}_{35}$, $\text{C}_{19}\text{H}_{39}$, $\text{C}_{21}\text{H}_{42}$. Metallic Ag production in such a system further accelerates the development reaction via an autocatalytic reaction. In typical autocatalytic development,⁴ density formation depends on product concentration as well as on specific reactant concentrations, Eq. 1.

$$\frac{dX}{dt} k_{\text{auto}} [A_0 - X] [X - X_0] \quad (1)$$

In this equation, k_{auto} is the autocatalytic rate constant, A_0 is the reactant concentration (e.g. Ag^+ concentration), X_0 is related to the latent image, and X is the product of the development reaction. The integrated

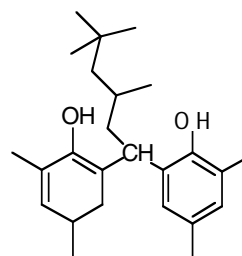
form of Eq. 1 provides a direct relationship between the product X , which is related to density, and k_{auto} , Eq. 2.

$$X = \frac{A_0 X_0 [e^{k_{\text{auto}} t (A_0 + X_0)} - 1]}{A_0 + X_0 e^{k_{\text{auto}} t (A_0 + X_0)}} \quad (2)$$

Another possibility is that the rate of reaction depends on the concentration of two components,⁵ such as the developer and the organic Ag compound, Eq. 3.

$$dX = k_{\text{auto}} (A_0 - X) (X + X_0) (rA_0 - X/4) dt \quad (3)$$

In Eq. 3, $A_0 - X$ represents the effective Ag^+ concentration, X and X_0 are the Ag metal, and $rA_0 - X/4$ is the effective developer concentration for a four-electron developer, such as the hindered bisphenol Nonox WSO, present at an initial ratio, r , to the Ag^+ .



Nonox

Equation 4, the integrated form of Eq. 3, cannot be explicitly solved for X .

Original manuscript received December 4, 1998

▲ IS&T Member

This paper was presented at IS&T's 50th Annual Conference, Cambridge, MA, May 18–23, 1997.

© 1999, IS&T—The Society for Imaging Science and Technology

$$k_{auto}t = 4 \frac{\text{Log}[(A_0 - X) / A_0]}{(A_0 - 4rA_0)(A_0 + X_0)} +$$

$$k_{auto}t = 4 \frac{\text{Log}[(A_0 - X) / A_0]}{(A_0 - 4rA_0)(A_0 + X_0)} + \quad (4)$$

Photothermographic Ag forms at the surface of pre-existing Ag, either Ag from the latent image or Ag from prior development. Density formation that depends on Ag surface area⁶ would increase less rapidly than density formation which depend on Ag mass, Eq. 5.

$$dX = k_{auto}(A_0 - X)(X + X_0)^{2/3}dt \quad (5)$$

In Eq. 5, all variables are the same as described above. Equation 6 gives an implicit solution to Eq. 5 for $X_0 \ll A_0$.

$$k_{auto}t = \frac{1}{2A_0^{2/3}} \left(\begin{array}{l} -2\sqrt{3}\text{Tan}^{-1} \left[\frac{A_0^{1/3} + 2X_0^{1/3}}{\sqrt{3}A_0^{1/3}} \right] + 2\sqrt{3}\text{Tan}^{-1} \left[\frac{A_0^{1/3} + 2(X + X_0)^{1/3}}{\sqrt{3}A_0^{1/3}} \right] + \\ 2\ln[A_0^{1/3} - X_0^{1/3}] - \ln[A_0^{2/3} + A_0^{1/3}X_0^{1/3} + X_0^{2/3}] + 2\ln[A_0^{1/3} - (X + X_0)^{1/3}] + \\ \ln[A_0^{2/3} + A_0^{1/3}(X + X_0)^{1/3} + (X + X_0)^{2/3}] \end{array} \right) \quad (6)$$

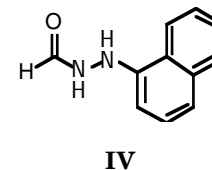
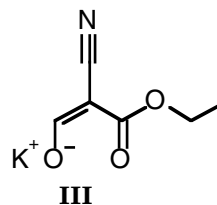
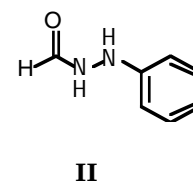
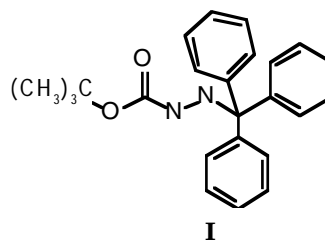
The standard development process provides the capability to initiate other reactions such as those responsible for high contrast infectious development. High contrast is preferred for halftone/text applications, such as imagesetting. In these systems the infectious developer may be a trityl hydrazide (I),⁷ a formylarylhydrazine (II, IV),⁶ or an acrylonitrile (III).⁸ Ag soaps containing infectious developers typically require significantly less Ag to reach a given density than films without infectious developers.

In parallel development all crystals form at the same time, while in sequential development the Ag particles form at different times.⁹ Because all the crystals develop at the same time in parallel development, the slope of the overall development curve will reflect the development of individual Ag particles. This slope does not depend on exposure. On the other hand, in sequential development the slope of the overall development curve will be dependent on exposure. In this case the development curve has no direct relationship to the formation of any single Ag particle. Parallel development is characteristic of Lith development while sequential development is characteristic of standard development.⁹

In this article, I report the kinetic and thermodynamic behavior of several photothermographic systems, including systems containing infectious developers. In these systems, the thermal development process was monitored spectrophotometrically. In addition, I will describe the morphology, size distribution, and optical properties of the resulting Ag particles.

Experimental

Kinetic Measurements. A 3M Model 179 Contact Printer-Processor was used to provide a blanket exposure. Development took place in a thermostated fluorochemical bath at 90–150°C. During development the film was protected from further development with a



1000 nm band pass filter. All kinetic measurements represent the average of at least three separate experiments. Nonlinear regression with Grafit gave optimized fits to theoretical rate equations. The regression included only data prior to the maximum experimental density to reduce the effect of aggregation on the analysis. Samples for electron micrographs were cryomicrotomed to a thickness of 85 ± 5 nm. Image analysis was completed with SigmaScan Pro. All sensitometric measurements used a laser sensitometer.

Results and Discussion

Silver Morphology. Photothermographic development takes place in either a noninfectious or infectious manner. The resulting Ag morphology is highly dependent on the mode of development, Fig. 1 and Table I.

Median Ag particle diameter decreases from $0.065 \mu\text{m}$ to ca. $0.03 \mu\text{m}$ in the presence of infectious developers. Median area decreases in a similar fashion. The smaller particle size correlates to the larger number of sites for Ag reduction.

Diffusion of a fogging agent to nearby Ag soap results in the formation of secondary development sites during infectious development. In the presence of infectious developers, the "sphere of influence"³ of each Ag halide grain will depend more on the diffusion of fogging agent away from the grain than on the diffusion of Ag^+ to the grain. In the absence of infectious developers, nucleation sites are limited to the Ag halide.

Ag particle size directly affects light absorption. Standard photothermographic systems show absorption that is independent of wavelength, while high contrast systems have significant reduced absorption at wavelengths greater than 800 nm, Fig. 2. Ag particles smaller than those particles formed through infectious development would not have a neutral image tone.

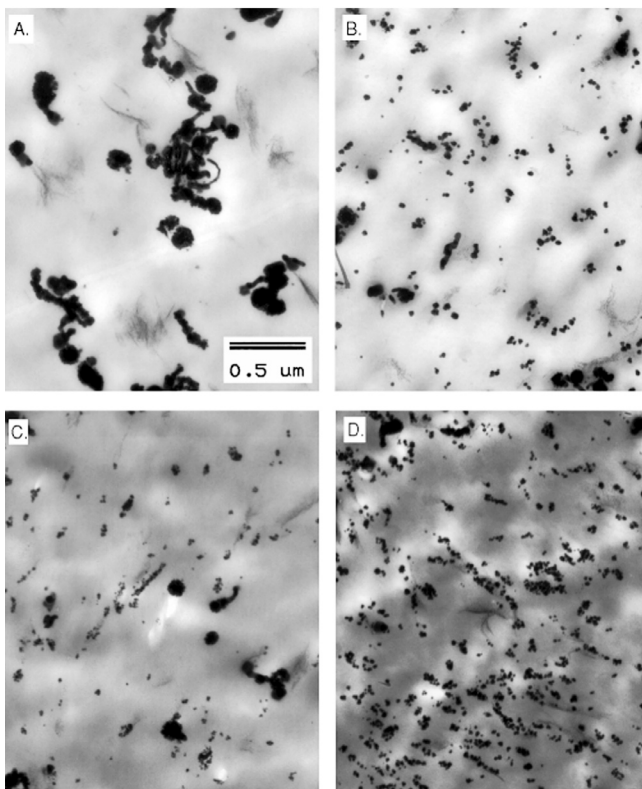


Figure 1. Ag morphology of photothermographic films containing no infectious developer (A), II (B), I (C), and III (D).

Intermediate levels of infectious developers give an intermediate level of infectious development, Fig. 3. In this situation, median particle size falls between median particle sizes for systems that show conventional and systems that show infectious characteristics.

Development Kinetics. Density changes during development reflect the kinetics of the underlying chemical processes. Development typically requires a temperature of at least 90°C. Spectrophotometric observation of film development is then possible at observation wavelengths that are outside the film's region of sensitivity. An observation wavelength of 1000 nm is sufficiently far removed for films sensitized to 800 nm. For exposed films, a blanket exposure provides the required latent image for thermal development. If the film is not exposed, density changes during thermal processing reflect both fog and non-photothermographic Ag reduction.

A typical plot of density versus time (120°C) has a sigmoidal shaped development curve, Fig. 4. Development consists of an initial induction period, rapid autocatalytic development, a shoulder with reduced development rate as reagents are depleted, and a final time period which may include loss of density. At the completion of standard development, some unreacted Ag soap is typically present.

Fits of experimental data in Fig. 4 to autocatalytic rate equations show that Eq. 2, in which rate depends on the product and one reactant, best describes the observed data. Greater deviation from the observed data is observed for Eq. 4, which incorporates both the Ag⁺ and the developer, and for Eq. 6, which incorporates the surface area of the resulting Ag. Consequently, Eq. 2 was used for analysis of kinetic data.

TABLE I. Size and Morphology of Ag Particles from Various Photothermographic Systems

Sample	DryView	I	II	III	IV ^c
Average Shape ^a	0.69	0.79	0.77	0.79	0.50
Median Feret D (μm) ^b	0.065	0.023	0.028	0.035	0.050
Median Area (μm^2)	0.0033	0.0004	0.0006	0.0009	0.0019

^a Shape is defined as $4\pi A/P^2$, where A is the Area and P is the Perimeter. By definition, Shape is 1 for a circle and 0 for a line.

^b Feret D is the diameter of a circle in μm with a cross sectional area equivalent to the particle of interest.

^c Low level of infectious developer.

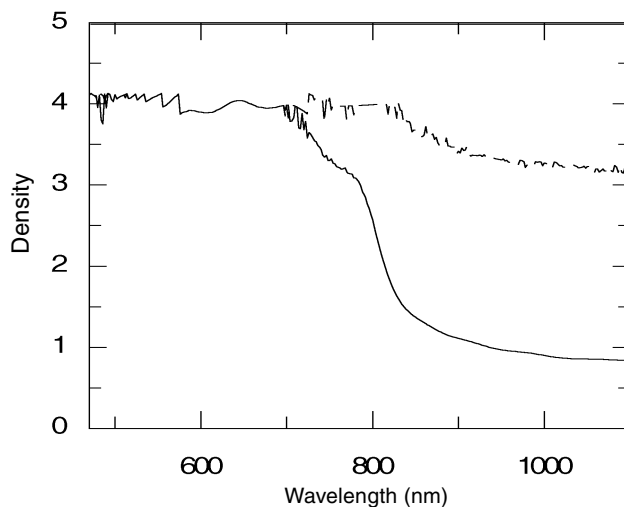


Figure 2. Spectral absorption of high contrast (solid line) and standard (dashed line) DryView photothermographic films.

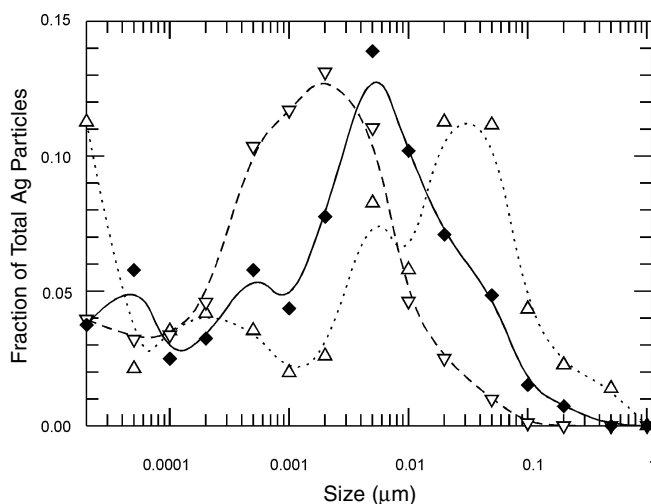


Figure 3. Size distribution as given by the Feret Diameter of Ag particles for standard development (Δ , Contrast = 4–5), high contrast infectious development (∇ , Contrast > 20), and low contrast infectious development (\blacklozenge , Contrast ~ 6).

Note that in these equations, the initial product concentration greatly exceeds the product concentration that could reasonably be expected from the latent image, which must be the initial source of autocatalytic

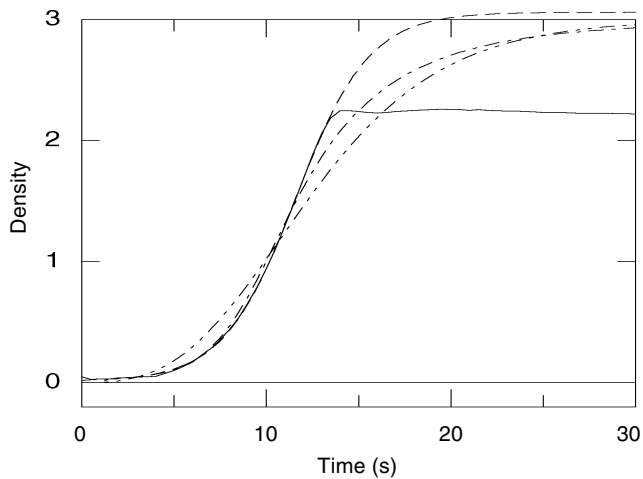


Figure 4. Plot of density versus time illustrating sigmoidal shaped development curve. Fits of experimental data to autocatalytic rate equations are shown for Eq. 2: $k_{\text{auto}} = 0.17$, $X_0 = 0.0084$, $A_0 = 3.04$ (—); Eq. 4: $k_{\text{auto}} = 0.21$, $X_0 = 0.0040$, $A_0 = 2.95$ (---), and Eq. 6: $k_{\text{auto}} = 0.11$, $X_0 = 0.00006$, $A_0 = 3$ (-·-·-).

reactivity. Consequently, the photothermographic latent image centers must be significantly more reactive than would be expected from simple extrapolation of the autocatalytic rate equation.

Kinetic behavior at different temperatures for systems with and without infectious developers shows striking differences as shown in Fig. 5. Standard development shows good correlation to Eq. 2 for all temperatures for both unexposed and unexposed samples, as in Figs. 5A and 5B. The greatest deviation is apparent at high density and at long processing times. At high densities, density may not accurately describe the amount of Ag present. In addition, processes other than Ag development may predominate at greater processing times.

Infectious development shows significant deviation from predicted behavior as seen in Figs. 5C and D. Most notably, density decreases significantly at long development times. For example, median Ag particle diameter as determined from electron micrographs increases from 0.026 to 0.039 μm , yet total Ag coverage decreases from 45% to 36% when development time is increased from 7 to 25 s. This decrease in coverage results from the aggregation of smaller Ag particles to larger clusters with reduced covering power.

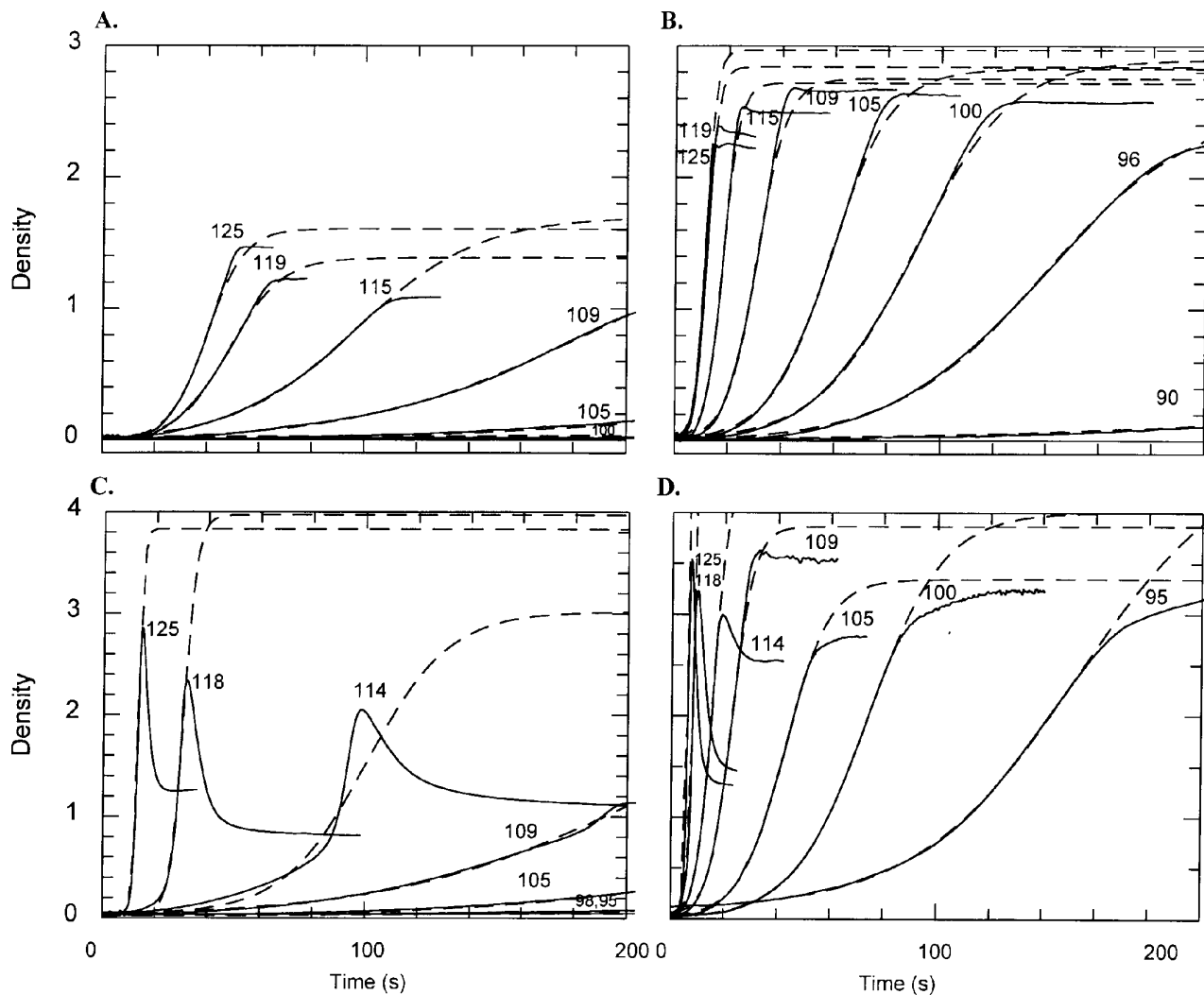


Figure 5. Development kinetics for unexposed (A) and exposed (B) standard films and for unexposed (C) and exposed (D) infectious development films.

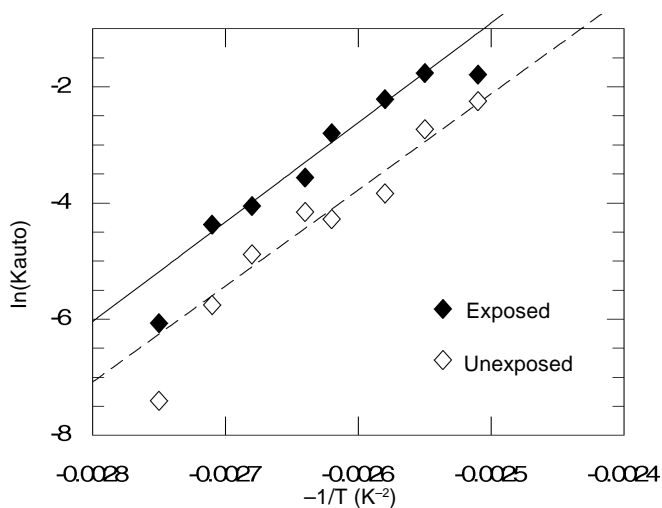


Figure 6. Determination of thermodynamic parameters for photothermographic development.

In addition the data for certain temperatures, such as for unexposed film at 114°C, deviates significantly from predicted behavior during initial Ag formation as shown in Fig. 5C. The complicated nature of the chemical reactions in systems containing infectious developers has so far prevented complete analysis of the development kinetics.

Photothermographic Thermodynamics

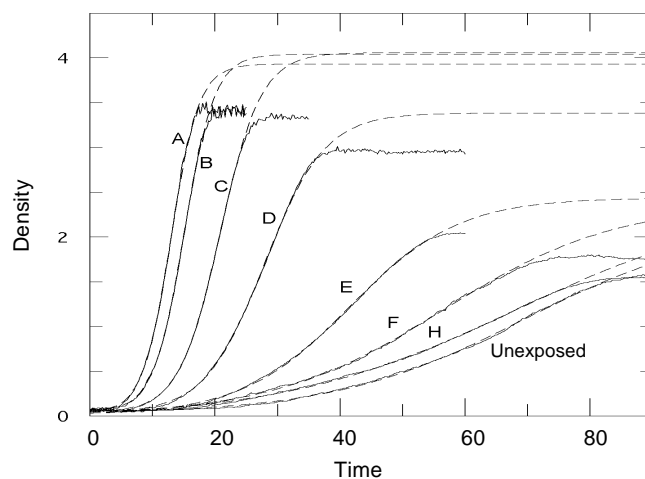
The slope, Ea/R , of the Arrhenius plot¹⁰ of $\ln(k_{\text{auto}})$ versus $-1/T$ is identical for exposed and unexposed photothermographic samples within experimental error, as seen in Fig. 6. Consequently, the enthalpy of activation, ΔH^\ddagger , which is $Ea - RT$ from transition state theory is also identical for the two samples. On the other hand, the intercept of the Arrhenius plot, $\ln(A)$, where A is the preexponential factor, is significantly different. From transition state theory A is $(ek_B T/h)e^{\Delta S^\ddagger/R}$, where ΔS^\ddagger represents the entropy of activation and e is 2.718.

For the unexposed film and exposed films, Ea is 8.3 ± 0.8 and 8.8 ± 0.8 Kcal/mole, ΔH^\ddagger is 32 ± 3 and 34 ± 2 Kcal/mole, and ΔS^\ddagger is 17 ± 8 and 23 ± 6 cal/mole \cdot K⁻¹, respectively. The similarity of these thermodynamic parameters suggest that similar mechanisms operate for developing fog and image centers in standard photothermographic films.

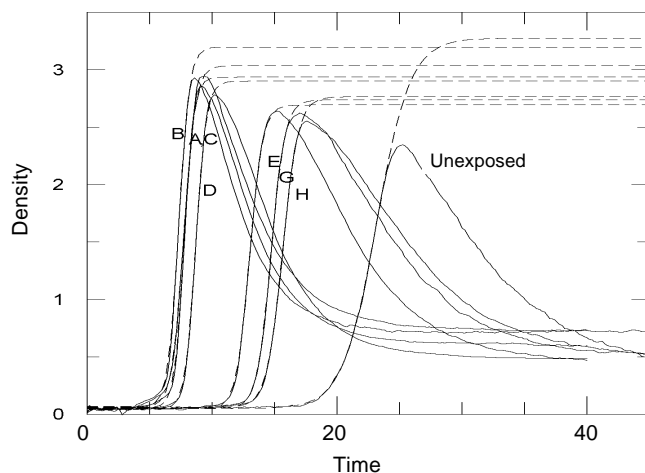
The positive ΔS^\ddagger for photothermographic development indicates rate determining step contains a unimolecular transition state. If the transition state were bimolecular, ΔS^\ddagger would be large and negative, reflecting loss of entropy in the transition state. This thermodynamic observation is consistent with the fact that an autocatalytic rate equation with only one chemical species best describes the development kinetics.

A unimolecular transition state is only possible if the necessary reactants are present as a preexisting complex. Under these conditions, the rate determining step would then involve electron transfer within the preexisting complex.

Effect of Exposure. The rate of development for standard photothermographic film is dependent on exposure (Fig. 7A). For these films the linear portion of the development curve has a greater slope at higher exposure levels. Formation of individual Ag particles takes place sequentially. On the other hand, films containing



(a)



(b)

Figure 7. Dependence of standard development (A) and infectious development (B) on exposure. Blanket exposure (8.5 s) was through a neutral density step wedge with densities of 0.067, 0.48, 1.00, 1.52, 1.97, 2.50, 3.08, 3.21 for exposures A through H, respectively.

infectious developers have development curves with a slope that does not depend on exposure (Fig. 7B). Infectious development of Ag halide grains takes place in parallel. Films containing infectious developers that are not exposed do, however, develop less rapidly than exposed films. This apparent dichotomy suggests that fog development and photothermal development operate via different mechanisms in these films.

The maximum density of standard DryView photothermographic films increases with increasing multiple exposures (Fig. 8). The increased density is primarily due to an increase in the number of particles, as the median particle size remains unchanged (Fig. 9). D_{max} increases 26% from 3.63 to 4.57, and the number of particles increases 32% from 5.62 to 7.37/ μm^2 . With 50 exposures, the only apparent morphological change is that the largest Ag particles ($A > 0.05 \mu\text{m}^2$) are significantly less spherical. These particles have a compactness ($\text{Perimeter}^2/\text{Area}$) of 64 rather than 48, and shape ($4\pi \times \text{Area}/\text{Perimeter}^2$), which ranges from 0 for a line to 1 for a circle decreases from 0.32 to 0.23.

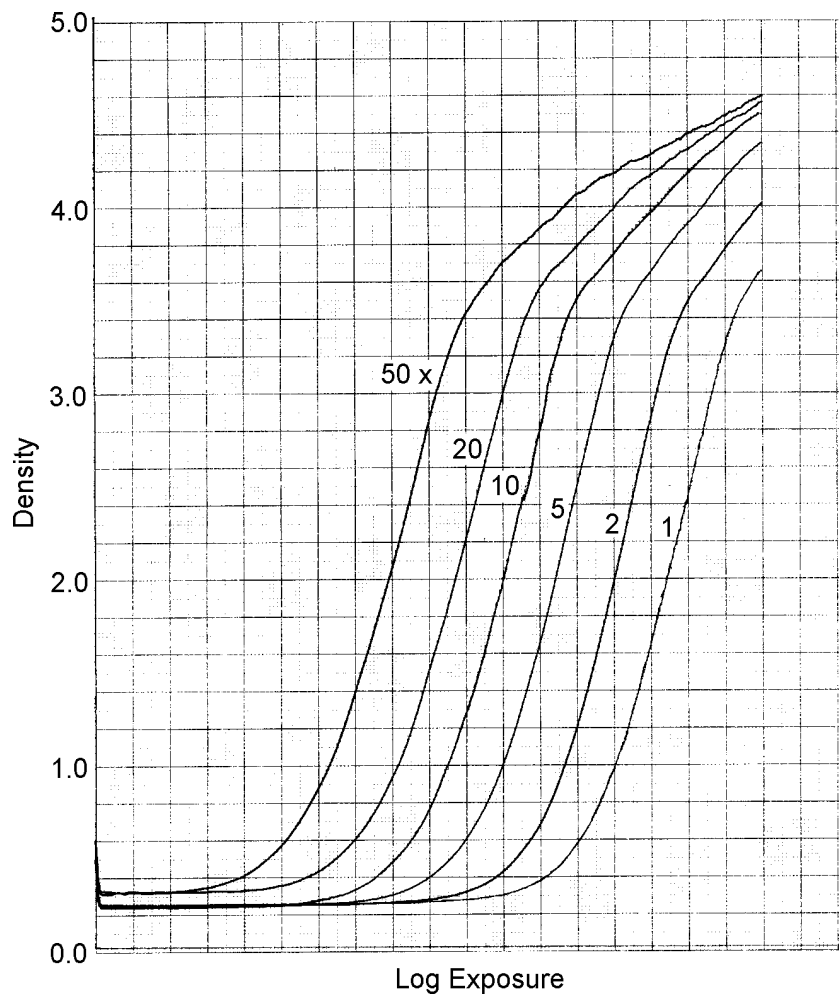


Figure 8. Changes in the characteristic curve of DryView with repeated exposure. Curve 1 represents one standard DryView exposure; curve 50 represents 50 exposures in succession repeated at a rate of approximately 1/s.

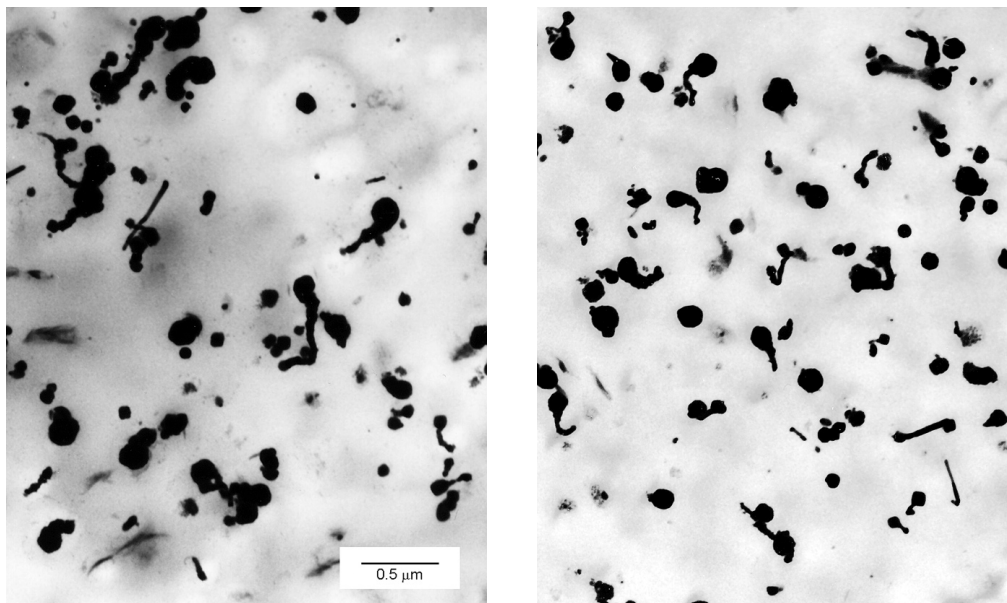


Figure 9. Ag morphology at maximum density for a single exposure (A) and for 50 exposures in succession (B).

Conclusions

The addition of infectious developers to photothermographic systems greatly changes the course of development. Standard photothermographic development follows the sigmoidal, autocatalytic rate equation. For these films, thermodynamic parameters are similar for unexposed and exposed samples. The entropy of activation suggests a unimolecular transition state in the rate determining step for films without infectious developers. Infectious development follows more complicated kinetics. Particle size is smaller and covering power is higher in the presence of infectious developers.

Different kinetic models describe each development system. Standard development is sequential, while infectious development occurs in parallel. Parallel development in the presence of infectious developers results in significantly smaller Ag particles. Intermediate levels of infectious developers result in intermediate particle sizes. 

Acknowledgments. Nancy Grace and Marcie Moller assisted with the kinetic measurements. Wenyuan Xu (3M) provided helpful discussion of the relevant rate equations. Russ Isbrandt and Sharon Simpson prepared

the photothermographic samples. Mary Buckett (3M) obtained the electron micrographs. Final thanks goes to the management at Imation Corp. for their support of this work.

References

1. C. Zou, J. B. Philip, S. M. Shor, M. C. Skinner, and P. Zou, U. S. Patent 5,434,043 (1995)
2. S. M. Shor, Ultra High Contrast Photothermographic Media and its Potential Use in Graphic Arts Laser Applications, *Proc. IS&T 49th Annual Conf.*, IS&T, Springfield, VA, 1996, p. 442.
3. D. H. Klosterboer, in *Imaging Processes and Materials: Neblette's Eighth Edition*, J. Sturge, V. Walworth, and A. Shepp, Eds., Van Nostrand Reinhold, New York, 1989, pp. 279–291.
4. K. J. Laidler, *Chemical Kinetics*, McGraw-Hill, New York, 1965, pp. 1–30.
5. L. Kvitek, A. Julak and J. Straka, *Acta Univ. Palacki Olomuc., Fac. Rerum Nat.* **117**, 61 (1994).
6. J. R. Fyson and G. P. Levenson, *J. Photo. Sci.* **25**, 147 (1977).
7. a. S. M. Simpson and L. S. Harring, U.S. Patent No. 5,558,983 (1996); b. S. M. Simpson and L. S. Harring, U.S. Patent No. 5,496,695 (1996).
8. T. J. Murray and S. M. Simpson, U.S. Patent 5,545,515 (1996).
9. (a) T. H. James, in *The Theory of the Photographic Process*, T. H. James, Ed., Eastman Kodak, Rochester, 4th ed., 1977, pp. 373–436; (b) S.-X. Ji, F.-Y. Ma, P. Hu, and X.-M. Ren, *Ganguang Kexue Yu Kuang Huaxue (Photographic Science and Photochemistry)* **9**, 261 (1991).
10. T. H. Lowry and K. S. Richardson, *Mechanism and Theory in Organic Chemistry*, 3rd ed., Harper & Row, New York, 1987, pp. 190–228.